Materials Horizons

ROYAL SOCIETY OF CHEMISTRY

COMMUNICATION

View Article Online
View Journal

Cite this: DOI: 10.1039/d5mh00569h

Received 30th March 2025,
Accepted 7th July 2025

DOI: 10.1039/d5mh00569h

rsc.li/materials-horizons

Integrated iontophoresis and sweat sensing *via* paper-derived laser-induced graphene soft conductors†

Tomás Pinheiro, * Henrique Vazão de Almeida, Daniela Nunes, Rodrigo Martins and Elvira Fortunato *

The development of mechanically compliant, functional materials toward skin-integrated electronic systems has been a rapidly evolving field, aiming at flexible and even stretchable architectures that can be mounted into curved skin surfaces and adapt to their changing topography and biomechanics. One of the components required for functional bioelectronic systems is bioelectrodes that can robustly interact with the skin to perform sensing or stimulation tasks. In this work, paper-based laser-induced graphene is studied as a compatible material for skin-integrated systems for iontophoretic sweat stimulation and sweat metabolite sensing. Based on a water-induced peel-off strategy, robust transferred LIG soft conductors using polyurethane film substrates were fabricated and characterized, showing a compatible electrical conductivity of 29.3 S cm^{-2} and a high graphitization yield, confirmed by scanning transmission electron microscopy and Raman spectroscopy. Based on these results, paper-based, transferred LIG/PU bioelectrode architectures were used to develop iontophoresis stimulation systems for the delivery of cholinergic agents and sweat secretion activation. The delivery of carbachol as a model cholinergic agent was studied, demonstrating the capability of stimulating up to 60 μL of sweat with a 10-minute stimulation period, over a period of 1 hour. The iontophoresis system was also integrated with a flexible LIG-based enzymatic glucose sensor, showing a high sensitivity of 29.73 μA mM^{-1} cm^{-2} and a limit of detection of 5.45 μM, capable of distinguishing glucose levels at fasted and post-prandial states, using more sustainable materials and resource-efficient fabrication, towards non-invasive sweat metabolite quantification.

New concepts

We present a novel route to skin-integrated electronic systems using paper-based laser-induced graphene (LIG) for iontophoretic sweat stimulation and metabolite sensing. Through a water-induced peel-off strategy, we fabricated robust LIG soft conductors on polyurethane, achieving excellent electrical conductivity and high graphitization yield. Our approach includes developing paper-based LIG/PU bioelectrode architectures for iontophoresis, enabling the delivery of cholinergic agents like carbachol to stimulate sweat secretion. Additionally, we integrated this with a flexible LIG-based enzymatic glucose sensor, demonstrating high sensitivity. This integrated sensing system effectively distinguishes glucose levels in fasted and post-prandial states, using conscious materials and efficient fabrication methods, enabling more sustainable fabrication and future deployment of non-invasive sweat metabolite sensing systems in different areas of the world.

1. Introduction

Bioelectronics has emerged as a robust technology, anchored on ongoing research on materials that combine several key features, such as mechanical flexibility with robust compliance, stretchability, biocompatibility, adhesion to tissue surfaces and breathability.[1,2] To achieve this, several material classes have been studied to develop soft conductors that can simultaneously participate in charge conduction and robustly adhere and adapt to biological tissue surfaces.[3] These include metal conductors, in the form of thin films, fillers or liquid metals,[4–6] conducting polymers,[7] hydrogels[8] and carbon nanomaterials.[9] Beyond materials, considerate shapes and form-factors also aid in achieving conformability, including substrates with nature-inspired adhesive surfaces[10] or conductive serpentine or kirigami conductive material architectures.[3] Material innovations paired with their integration in functional systems have allowed bioelectronics to meet several requirements for biomedical device development.

For diagnostics, wearable bioelectronic devices have enabled the collection of useful physiological information that can be

CENIMAT/i3N, Departamento de Ciência de Materiais, Faculdade de Ciências e Tecnologia, Universidade Nova de Lisboa and CEMOP/UNINOVA, Campus da Caparica, 2829-516 Caparica, Portugal.
E-mail: tp.pinheiro@campus.fct.unl.pt, emf@fct.unl.pt

† Electronic supplementary information (ESI) available. See DOI: https://doi.org/10.1039/d5mh00569h

integrated within a diagnostic criterion for several complications. For biochemical-based diagnostics, the staple consumer wearable bioelectronics product has been continuous glucose monitors (CGMs), used in the management of diabetes mellitus. These are based on minimally invasive, hypodermic needle-based systems that measure glucose levels in circulating interstitial fluid. Using electrochemical transduction, needles are modified to serve as bioelectrodes for signal generation, based on enzymatic reactions.[11] Recently, alternative devices have been researched to decrease the invasiveness of CGMs. These include microneedle-based devices, which operate on similar principles to current CGMs,[12] or patch-like electronic skin (e-skin) devices that can access sweat as a biological fluid matrix, where glucose can be sampled and measured through electrochemical transduction.[13] Most notably, enzymatic glucose sensors have demonstrated their capability for detection of glucose in different physiologically relevant orders of magnitude, from the millimolar levels characteristic of blood (2–40 mM) and interstitial fluid (2–22 mM) to the micromolar level characteristic of sweat (10 μM–1.11 mM), by careful selection of biosensing schemes and highly sensitive mediators, showing an increasing acceptance for wearable biochemical sensor development.[14] Furthermore, such types of devices have been increasingly investigated for the measurement of different analytes in sweat for several diagnostic and prognostic purposes, such as for cystic fibrosis,[15] kidney function,[16] gout,[17] inflammation[18] or human stress response,[19] strengthening the knowledge and interest in the potential use of sweat as a valuable diagnostic source.

Regarding the fabrication of skin-interfaced bioelectronics, direct laser writing (DLW) has increasingly been selected as a route to synthesize and pattern low-thickness, conductive, flexible geometries from several material precursors, aiming at different functions, from electrophysiology applications to on-skin biochemical detection.[20] An example is the patterning of molybdenum dioxide (MoO_2) from a metal salt precursor, to develop bioelectrodes for different applications, including on-body temperature sensing, ECG signal acquisition, UV photodetectors and biochemical sweat sensors for glucose, uric acid and caffeine detection. For the glucose sensor, a sensitivity of 15.7 nA μM^{-1} was achieved. Another example is the use of laser carbonization to pattern conductive carbon materials as bioelectrodes. In the work by Sharifuzzaman *et al.*,[21] a MXene/fluoropolymer substrate was used as a precursor to write bioelectrodes for sweat glucose sensing and ECG acquisition. The enzymatic sweat sensor presented a sensitivity of 77.2 μA mM^{-1} cm^{-2}, a linear range between 10 μM and 2 mM and a limit of detection of 10 μM. Based on laser-induced graphene (LIG), several examples of highly efficient sweat glucose biosensors have been reported, based on different precursors, including PI,[22–28] PES[29] and lignin.[30] Regarding the biodetection mechanisms, most sensors rely on ultrasensitive elements that can very efficiently oxidize or reduce hydrogen peroxide (H_2O_2) and generate amperometric signals in the presence of low glucose concentrations, mostly relying on platinum nanoparticles (PtNPs) for this purpose.[22,25,28] Alternative mechanisms include highly sensitive mediators, such as Prussian Blue[30] and nonenzymatic methods, using transition metal nanostructures, such as copper or nickel.[26] Most of these reports have been employed in *in vivo* scenarios[22–25] or tested with collected sweat samples,[27,28,30] demonstrating their capability for integration in bioelectronic systems for sweat metabolite sensing. While most of these sweat glucose biosensors have been tested *in vivo* by sweat induction through physical exercise, the fabrication of LIG-based iontophoresis systems for sweat induction has been recently demonstrated. This allows for a single step fabrication of all the required bioelectrodes for sweat induction and sensing in a single PI chip substrate, for controlled sweat induction and prolonged sweat sensing towards high-frequency sampling and continuous analysis.[18,31] However, in the pool of precursor materials, petroleum-based polymers, mainly PI, have been the main research focus, while naturally available, more abundant materials lack behind in technological implementation stages. In this work, paper-derived LIG is used for the fabrication of skin-interfaced bioelectrodes, towards flexible, wearable biosensing. Based on laser processing approaches, complex bioelectrode geometries and their assembly with seamless integration strategies are demonstrated to develop robust e-skin patches for biochemical sweat analysis, towards biomedical diagnostic devices. Paper-based LIG electrodes were tested as an anode and a cathode within an iontophoresis system for the stimulation of sweat, using the delivery of the slowly metabolized cholinergic agent carbachol.[32] The principles for sweat secretion stimulation using these electrodes were studied with respect to the stimulation current, resulting carbachol delivery, sweat rate and secreted volume. As a proof-of-concept, sweat glucose detection was attempted, by development and integration of a high-sensitivity enzymatic glucose sensor, constructed over flexible LIG-based electrochemical cells. A first *in vivo* test of the integrated device was performed with one subject, by measuring the current response of the sensor when exposed to stimulated sweat at a fasted state and after a meal.

2. Results and discussion

2.1. Fabrication and characterization of LIG soft conductor electrodes

LIG generation using more sustainable and abundant precursor materials is increasingly gaining preponderance in functional device development, including in wearable electrochemical sensing. Exploiting previous findings, chromatography paper substrates (Whatman grade 1, 180 μm thickness, 11 μm pore size, and 48% porosity) treated with sodium tetraborate and coloured paraffin wax are used in this work as a highly efficient graphitizable substrate, capable of producing highly conductive LIG films comparable to synthetic aromatic polymers. This can be done by tailoring substrate composition and laser conversion parameters, as previously demonstrated in dedicated laser processing-LIG property

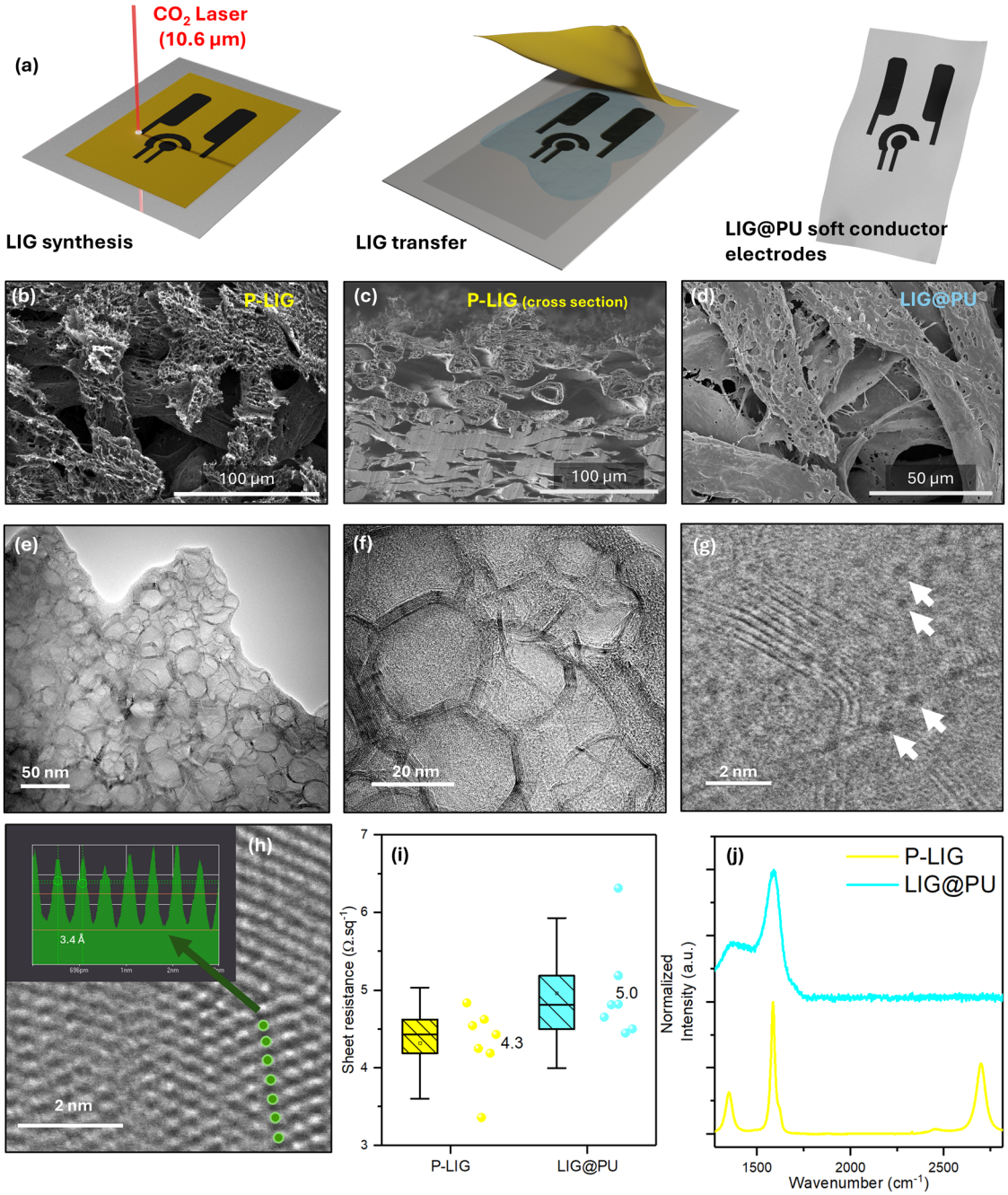

Fig. 1 Fabrication and characterization of LIG and LIG@PU soft conductor films. (a) Scheme of LIG synthesis and patterning, water-induced peel-off transfer and resulting LIG@PU soft conductor geometries. (b) SEM micrograph of the P-LIG surface, (c) cross-section and (d) LIG@PU surface. (e) and (f) BF-TEM images of LIG flakes after sonication. (g) and (h) Atomic-resolution BF-STEM images of the crystalline graphitic layers. The arrows in (g) point to the atomic structural features usually observed in LIG flakes, and the line profile in (h) was acquired from the carbon atoms indicated. (i) Sheet resistance and (j) Raman spectroscopy analysis of P-LIG and LIG@PU.

correlation studies.[33] In this work, a double lasing protocol using 6 W laser power and an engraving speed of 152.4 mm s^{-1} were employed, using a commercial CO_2 laser engraver (full experimental details are provided in the ESI†). With these laser synthesis parameters, improvements are achieved regarding the graphitization yield and electrical resistivity. With the resulting paper-based LIG, dedicated transfer protocols further increase its use cases in functional wearable applications. The fabrication process of LIG@PU soft conductors (Fig. 1a) is based on a water-induced peel-off method, in which laser-synthesized LIG functional geometries can be efficiently separated from the precursor substrate, by differential interaction of water with converted and unconverted phases. The cellulose precursor interacts and absorbs water, through hydrogen bonding, increasing its volume and promoting the detachment of converted LIG. When interfaced with an adhesive PU substrate,

anchoring of LIG geometries is possible, with water avoiding the bonding of the paper substrate and enabling its peel-off. This method can be used to fabricate distinct soft conductor electrode shapes and organizations, defined in the laser fabrication design process, tailored to specific functions. Furthermore, its encapsulation leads to mechanically stable and compliant soft conductive films, which can withstand the significant mechanical deformation characteristic of on-body operation, with a strain of up to 10%.[33] Full experimental details of the synthesis, transfer and characterization of LIG materials are presented in the ESI.† The first stage when surveying the capabilities of paper-based LIG (P-LIG) and its transferred soft conductor format (LIG@PU) for flexible, conformable bioelectrode development and iontophoresis device fabrication was to study different key properties, including surface morphology, chemistry and electrical conductivity, needed for efficient implementation within iontophoretic stimulation. SEM analysis of LIG surfaces was performed, to compare the morphology before and after transfer. For P-LIG (Fig. 1b), the fibrous structure of the precursor cellulosic substrate is retained after laser processing. As expected, laser-induced porosity is visible in the resulting LIG surface, mostly over more elevated cellulose fibers. Cross-section analysis of P-LIG was performed (Fig. 1c) to determine the thickness of the graphitized portion and the subsequent LIG@PU layer after transfer. As can be seen, the top portion of the paper substrate is graphitized, showing an increase in fiber porosity within the laser graphitized depth, without damaging the fibrous cellulose structures. Furthermore, incorporated wax is decomposed after irradiation, as visible by the empty inter-fiber volume. The thickness varies slightly over the extension of the P-LIG film, depending on cellulose fiber organization, at around 80 μm. For LIG@PU (Fig. 1d), SEM imaging shows less porous fiber structures, arising from the inversion of the material surface after transfer. Although the LIG surfaces before and after transfer are not directly interfaced with the skin when employed in the iontophoresis and electrochemical sensing systems, the smoother surface is more stable when interfacing and transmitting the current stimulus employed for iontophoretic stimulation. Additional STEM analysis was performed to analyze the atomic organization of the LIG's graphitic structure. In Fig. 1e, a fluffy morphology of LIG flakes can be observed, while Fig. 1f evidences their polycrystalline nature, characterized by ring-like and disordered structures, which are typical of graphitic nanomaterials. The rippled and turbostratic nature of the layered graphene structure is attributed to the thermal expansion caused by the laser irradiation.[34] Previous studies have reported that the flakes have a partially amorphous/partially hexagon lattice structure with heptagon–pentagons pairs.[34,35] A similar amorphous-like structure with fine structural features was also observed (Fig. 1g). Moreover, within the ring-like structures, an average lattice space of ~3.4 Å was measured (Fig. 1h), which corresponds to the (002) planes of graphitic materials (the line profile of the C atoms in the inset).[34,36]

Regarding the electrical conductivity, sheet resistance measurements show single-digit values for both P-LIG and transferred LIG@PU (Fig. 1i). Previous laser processing-LIG property correlation studies have been conducted to reach low sheet resistance LIG films derived from paper, by tailoring the substrate composition and laser synthesis parameters.[33] For this study, improved synthesis parameters previously described provide not only for low sheet resistance, but improved the yield after transfer. P-LIG films prior to transfer showed a lower resistivity, at $4.3 \pm 0.4\ \Omega\ \mathrm{sq}^{-1}$ ($n = 7$). After transfer, LIG@PU shows a median sheet resistance of $5.0 \pm 0.6\ \Omega\ \mathrm{sq}^{-1}$ ($n = 7$), showing that there is a negligible effect of the transfer mechanisms towards the overall surface resistivity and 100% yield, with no transferred films portraying loss of function. Taking the cross-section length of LIG films from Fig. 1c, conductivities of $29.3 \pm 3.5\ \mathrm{S\ cm}^{-1}$ and $25.5 \pm 2.6\ \mathrm{S\ cm}^{-1}$ for P-LIG and LIG@PU were obtained, respectively. These values do not consider the porosity of cellulosic fibre structures and imposed by the laser, meaning that the intrinsic conductivity of the LIG is significantly higher than this apparent conductivity. Although their electrical conductivities, are similar, surface Raman spectroscopy analysis shows marked differences between P-LIG and LIG@PU (Fig. 1j). P-LIG shows distinctive D, G and 2D peaks, characteristic of graphene and graphitic materials, with a I_D/I_G peak intensity ratio of 0.25, demonstrating low defect density. Considering that the bulk of the aromatic content present in the precursor paper substrate is introduced by the wax treatment,[33] this is an exceptionally low value, portraying the efficacy of the modification strategy and the two-step, defocused beam irradiation protocol, leading to high efficiency graphitization. Taking the I_D/I_G ratio, the crystallite size in the a axis (La) was calculated for P-LIG, showing a very appealing values of 76.9 nm, comparable to the literature with aromatic polymer precursors.[37] For transferred LIG@PU, the inversion of the P-LIG film occurs, exposing a more amorphous carbonized material where G and D peaks show a broader width and the 2D peak is absent. This represents the decrease in graphitization efficiency with depth, resulting in a shift towards material carbonization at the farthest region affected by the photothermal conversion process. The absence of the 2D peak and broad D and G peaks shows that sp^2 clustering is still present, but the bulk of the surface is amorphous, although without detriments to the LIG soft conductor resistivity. With these properties, LIG@PU shows comparable electrical conductivity to LIG derived from other high-efficiency precursors, including aromatic polymers, compatible for the current application to the skin for iontophoretic delivery at different skin resistive loads, without the need for applying elevated electrical potentials (<10 V).[38]

2.2. LIG-based iontophoresis devices for sweat stimulation

An important function that a bioelectrode can perform is the electrical stimulation of biological tissues. It can have important biomedical applications, including the movement of charged and neutral molecules trough tissue barriers, by the action of electrical fields, for drug delivery applications. Transferred, LIG@PU electrodes were tested for this purpose, serving as iontophoresis electrodes for the delivery of the cholinergic

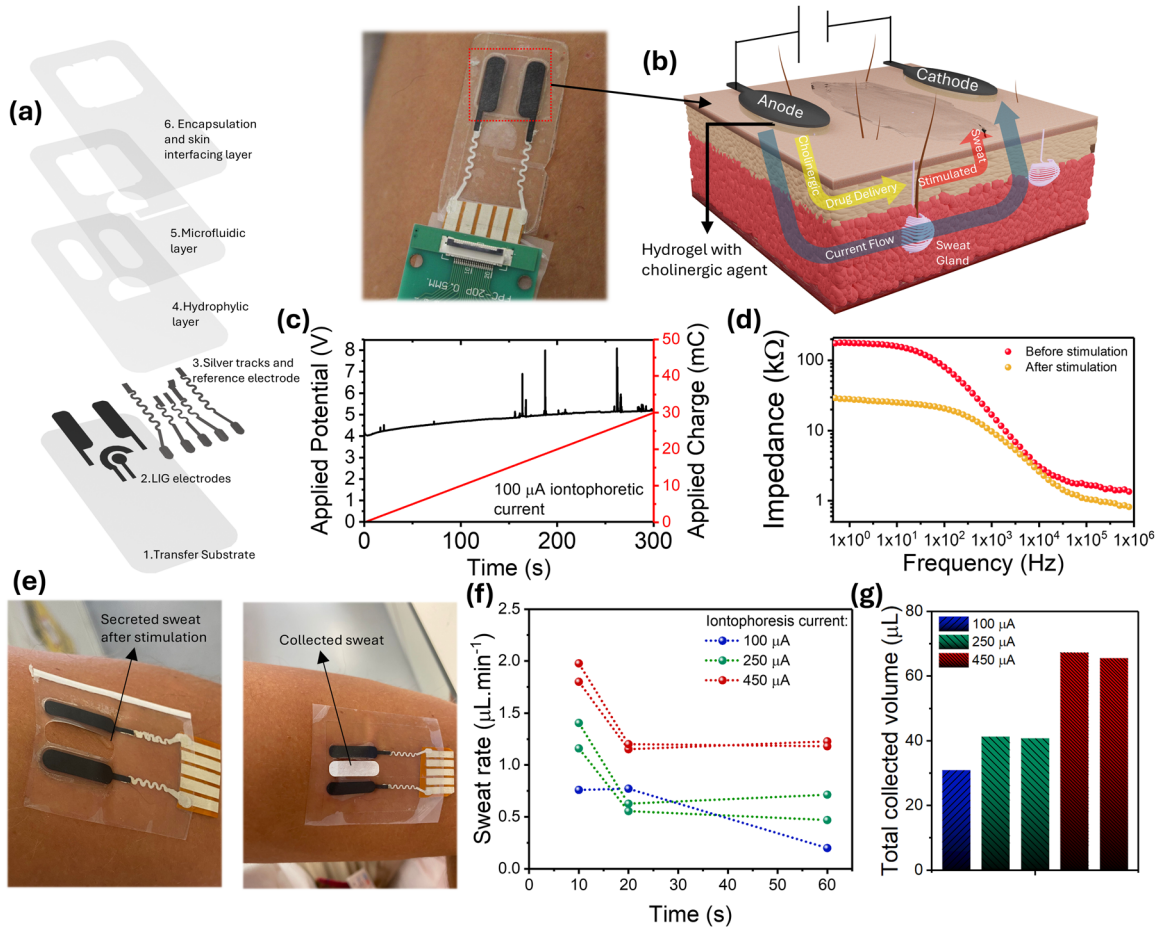

Fig. 2 LIG@PU-based iontophoresis patch for sweat stimulation. (a) Scheme of device components and assembly, placement in the skin. (b) Working principle of iontophoretic cholinergic agonist delivery for sweat stimulation. (c) Representative iontophoresis protocol, by the application of 100 μA and resulting potential and charge profile. (d) Electrode-skin impedance before and after the iontophoresis protocol. (e) Iontophoresis module for the sweat rate and volume estimation. (f) Sweat rate for the iontophoresis protocol with different stimulation currents and (g) total collected sweat volume.

agonist carbachol, targeting drug induced sweat secretion for metabolite biosensing purposes. A schematic representation of the LIG-based iontophoresis electrodes, integrated with an epifluidic module for sweat transportation and sweat electrochemical sensors for glucose quantification is portrayed in Fig. 2a. Two rectangular shaped electrodes with curved edges and an area of 0.6 cm^2 were patterned and transferred onto the PU substrate, followed by modular assembly of epifluidic and sensing components, depending on the experiments performed with the device. Overall, device components additionally comprise the three electrode electrochemical sensing module, with modified WE for glucose sensing, an encapsulating layer with hydrophilic properties and opening for iontophoresis and electrochemical sensing electrodes, a microfluidic channel layer and a final encapsulation layer that seals the microfluidic channel and allows for adherence of the device to the skin, as shown in the picture (device without the electrochemical sensing module, for visualization of the microfluidic channel). For connection with the current source providing the electrical stimulus for iontophoresis, a silver track connector fabricated on polyimide was also integrated with the device, for connection with a flexible flat cable connector.

The LIG-based iontophoresis module was individually tested, without electrochemical sensor integration, to evaluate its operation mode, carbachol delivery capabilities, sweat secretion outcomes and establish a stimulation protocol to be employed for *in vivo* experiments. In this regard, several parameters are of importance, regarding the current profile used for stimulation, the charge delivered to the skin, the drug delivery dose, effects on the skin, and outcomes related to resulting sweat secretion rates over time and overall sweat secretion volumes, conducive for efficient sweat sampling and measurement. A schematic representation of the iontophoresis process (Fig. 2b) depicts the steps involved in the sweat secretion stimulation, starting with the flow of current from the anode through the hydrogel and the skin, towards the cathode. The anode hydrogel contains a 0.5% (w/v) concentration of carbachol, which due to its positive charge, moves along the current path and onto the skin, until reaching eccrine sweat glands. At this stage, the binding of carbachol with acetylcholine

receptors promotes the secretion of sweat to the skin surface, where it can be collected.

For the stimulation protocol, DC current profiles were employed to assess the influence on generated sweat. Fig. 2c shows the voltage profile associated with an application of 100 μA current for 5 minutes, along with the charge delivered during this iontophoresis period. While the applied current is constant, the potential changes and stabilizes over time, associated with the resistive load of different layers and their interface, either from the hydrogel or the skin tissue layers. Furthermore, sudden peaks are visible, associated with motion artifacts caused by friction between the hydrogel and the skin. This implies that for a consistent current application over the stimulated skin area, tight adherence is required, so that charge does not flow through reduced areas, increasing current density and possible skin discomfort and lesion. For the charge, the constant applied current implies a linear increase in the delivered charge, accumulating for the stimulation period. Fig. 2d shows the effects of iontophoretic stimulation on skin-electrode impedance, demonstrating a significant decrease in impedance, associated with the secretion of sweat and higher hydration of skin tissues under the anode, along with the accumulation of charged molecules over the stimulated area.

A sweat collection protocol for sweat rate and secreted volume analysis was performed with devices comprising only the iontophoresis electrodes and an opening for sweat collection (Fig. 2e). With this opening, iontophoresis stimulation was followed by the placement of an absorbent paper pad in-between the electrodes, absorbing and collecting secreted sweat. To determine the effect of iontophoretic current, different currents were employed for a 10-minute stimulation period, using five devices, and secreted sweat volume was analyzed, to determine the sweat rate one hour after stimulation. The experimental iontophoretic currents, resulting charge and estimated carbachol dose are presented in Table 1.

Depending on the applied current, different current and charge densities are delivered to the area underneath the electrode. Regarding the current density, this is an important consideration regarding possible adverse effects to the skin, such as irritation and burns. Regarding the charge, it is directly related to the delivery and movement of charged molecules and can be used to estimate the amount of drug being delivered to the skin. Using the Faraday constant (F = 96 485 C mol^{-1}), the amount of electricity carried by one mole of electrons is represented, and considering the monovalent nature of carbachol, the theoretical carbachol weight being transported to the skin can be computed. According to previous reports of iontophoretic delivery, the presence of competing, small ionic species and other factors reduces the efficiency of delivery to around 30% of this theoretical value,[32] while other factors, such as cholinergic hydrogel concentration, also influence the delivery and sweat gland stimulation.[15] According to these considerations, estimated carbachol delivery of 35, 85 and 150 μg shows similar values to previous studies employing this cholinergic agent.[31,32]

Table 1 Iontophoretic current application protocols for sweat rate estimation

Current (mA)	Current density (mA cm^{-2})	Charge density (mC cm^{-2})	Estimated carbachol delivery (μg)
0.1	0.17	100	∼35
0.25	0.42	250	∼85
0.45	0.75	450	∼150

The resulting sweat rate profiles for the tested iontophoretic current doses are presented in Fig. 2f, showing the calculated sweat rate after the 10-minute stimulation period, 20 minutes and 1 hour after stimulation. As expected, the increase in current and associated higher carbachol delivery leads to an increase in sweat rate, consistent over time. For 100 μA current, tested in one device, a sweat rate of 0.8 μL min^{-1} was recorded after stimulation, dropping to 0.2 μL min^{-1} after 1 hour. For the 250 μA current, tested in two devices, sweat rates above 1 μL min^{-1} are observed after stimulation, also maintaining higher rates after 1 hour, at 0.5 and 0.7 μL min^{-1}. For the highest applied current of 450 μA, sweat rates approximating 2 μL min^{-1} are achieved, maintaining levels above 1 μL min^{-1} for the entire testing period. In terms of the total extracted sweat volume (Fig. 2g), a value of 31 μL was stimulated with a current of 100 μA, increasing to values around 40 and 65 μL for 250 and 450 μA. Although the sweat rates achieved with this paper-based LIG iontophoresis device being below other reports for carbachol delivery, that have reached values above 3 μL min^{-1},[31] the resulting sweat volumes are sufficient for efficient sweat sampling, using the microfluidic design presented in Fig. 2a, which has a volume capacity of 15 μL. Thus, these results show efficient sweat secretion stimulation for all the current values, with the capacity for manipulating the resulting sweat rates and volumes generated by the device. From these three conditions, a stimulation current of 250 μA was selected for proof-of-concept integration with epifluidics and glucose electrochemical sensing module. A stimulation current of 100 μA provided lower sweat volumes, that can vary between individuals, and not be sufficient to perform sweat sensing trials, while 450 μA is slightly above the 0.5 mA cm^{-2} current densities recommended for stimulation.

A comparison with different wearable devices for iontophoretic delivery of cholinergic agents is systematized in Table S1 (ESI†), containing important variables in the use of these devices, namely electrode materials, delivered cholinergic agents, iontophoresis current profiles and stimulation time. It also includes the resulting metrics of sweat stimulation for each report, either the generated sweat volume or the sweat secretion rate, exhibiting comparable performance of this LIG soft conductor-based iontophoresis system. With the approach presented in this work, the use of common metal-based electrodes (*e.g.* gold[15,39] or Ag/AgCl[40–42]) is avoided, while being a more accessible alternative to other approaches using carbon-based electrodes within the iontophoretic delivery system, such as carbon-coated polyimide[43] and polyimide-derived LIG.[31] Furthermore, the delivery system fabricated *via* paper-based

LIG soft conductors can be operated under analogous experimental conditions, regarding stimulation currents and time, providing comparable sweat stimulation metrics, more specifically in terms of generated sweat rates, important for efficient sweat sampling, and total sweat volumes, compatible for integration with microfluidics for sweat sampling and electroanalysis with sweat electrochemical sensors. In addition, further exploration and fine-tuning of the delivery system, regarding the cholinergic agonist concentration or stimulation current profiles, can further enhance these metrics, to approximate the highest recorded sweat generation capabilities, around 3 μL min^{-1} of sweat rate.[31]

2.3. Electrochemical sweat sensor characterization and integration for on-skin glucose monitoring

A highly sensitive electrochemical biosensor using enzymatic detection mechanisms was fabricated over LIG@PU flexible electrochemical cells for sweat glucose quantification. These three electrode planar cells have been previously characterized in terms of their charge transfer capabilities, showing high electrochemical surface area and fast electron transfer rate kinetics, while being tolerant for operation under different bending conditions and retaining their characteristics after multiple bending cycles, compatible for operation in curved skin surfaces.[33] A schematic representation of the construction of glucose sensors is presented in Fig. 3a, where the WE was functionalized using PtNP electrodeposition to introduce this catalytic material that promotes H_2O_2 oxidation and an associated amperometric signal. After electrodeposition, GOx was covalently bound to the carbon electrode surface through EDC/NHS coupling, serving as the biological recognition element for glucose detection. With this sensor functionalization protocol, a biodetection scheme based on glucose oxidation by GOx and its flavin adenine dinucleotide (FAD) structure initiates the reaction, leading to the consumption of O_2 to produce H_2O_2. H_2O_2 can then be oxidized by the surface bound PtNPs under a constant potential bias, being transformed back into O_2 and H_2O and releasing two electrons that generate the amperometric signal related to glucose levels in circulation over the WE surface. Before integration with the iontophoresis device, the sensor was tested, to determine suitable operation potentials, with a potential of 0.5 V being selected for the chronoamperometry experiments, due to lower noise levels and higher sensitivity when compared to lower potentials (Fig. S1a, ESI†). Sensor calibration was performed, using this potential and a standard PBS testing solution with a concentration of 100 mM. A stepwise addition protocol was followed, by spiking different volumes of this solution into the sensor environment, resulting in the increasing glucose concentration interacting with the modified working electrode. As can be seen from the sensor response curve in PBS (Fig. 3b), current steps associated with low glucose concentrations down to 5 μM are distinguishable from the background current, exhibiting its good sensitivity. Furthermore, a consistent current increase is

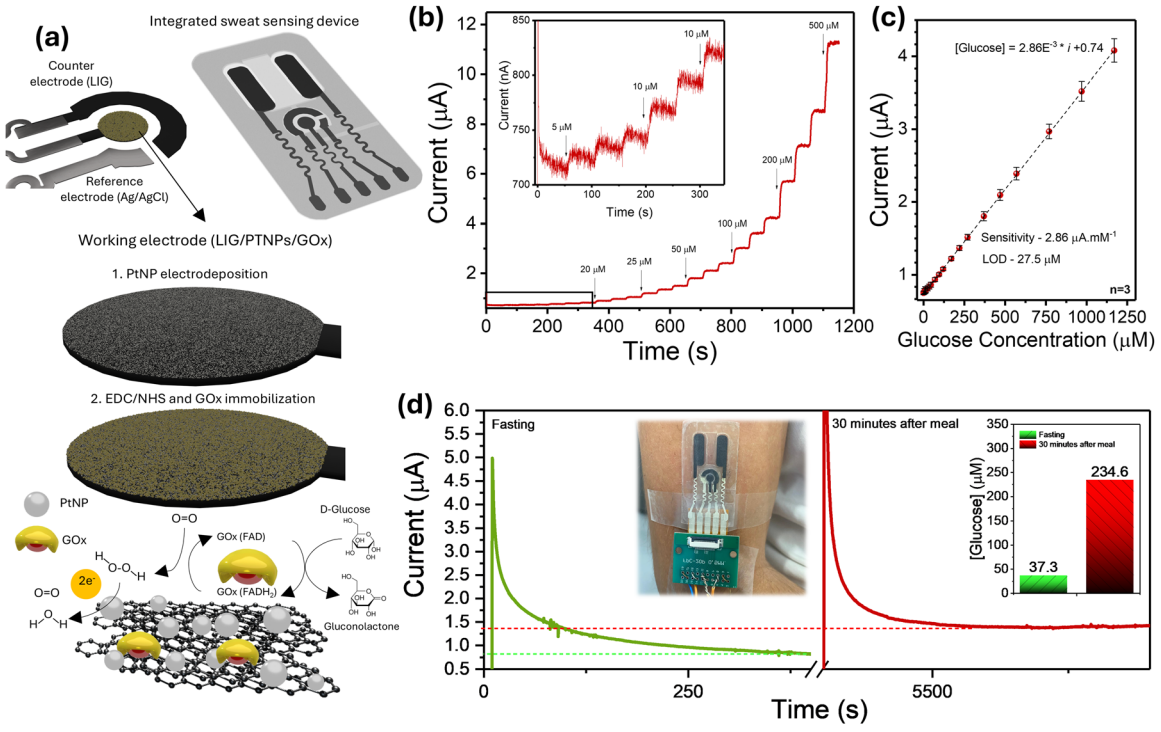

Fig. 3 Integrated iontophoresis and sweat glucose electrochemical biosensor system. (a) Scheme of the integrated iontophoresis device, electrochemical biosensor electrodes, modification strategy and biosensing scheme for sweat glucose detection. (b) Electrochemical sweat glucose sensor response curve and (c) calibration curve. (d) *In vivo* testing of the integrated iontophoresis device and resulting sensor response curve at a fasting state and after a meal.

achieved for each glucose concentration being added to the sensor, showing its great stability over continuous operation. To calibrate the sensors (Fig. 3c), current values taken after stabilization for each glucose addition step were plotted *vs.* the corresponding glucose concentration, for a batch of three sensors (n = 3). A resulting linear range between 5 μM and 1.17 mM was reached, with a sensitivity of 2.86 ± 0.2 μA mM^{-1} (29.77 ± 1.8 μA mM^{-1} cm^{-2}). With this sensitivity value, the LOD ($3.3\sigma/S$) was computed for each of the three individual sensors, resulting in values of 4.62, 5.98 and 5.76 μM (5.45 ± 0.6 μM). Due to the relatively high bias operation potential, interferent analysis was performed, by scoping the sensor response in a commercial eccrine sweat matrix, containing the most common metabolites (urea, uric acid, lactic acid and ammonia), electrolytes and amino acid in physiological concentrations. The results indicate no significant shift in the current response arising from their presence, both in the stepwise glucose addition, resulting in similar upward current shifts, and in the signal current difference for the same glucose concentrations (10 and 50 μM) when in a PBS and in spiked artificial sweat matrix (Fig. S1b and c, ESI†). Furthermore, the sensor calibration curve using this matrix results in a similar sensitivity value when compared with standard glucose solution in PBS buffer (2.86 μA mM^{-1} in PBS *vs.* 2.79 μA mM^{-1} in artificial sweat).

With these analytical parameters, the sensors show a compatible performance to detect and quantify physiological levels of glucose in sweat. Thus, sensor integration was performed, by assembling a sensor with the iontophoresis device and the epifluidic module, for delivery of stimulated sweat onto the surface of the sensing electrodes. A proof-of-concept *in vivo* measure was performed, with the integrated skin-worn device mounted laterally in the upper arm (Fig. 3d). First an iontophoresis sweat stimulation step (250 μA, 10 minutes) was performed, and an amperometric measure of sensor response was taken 5 minutes after the end of the stimulation period, to ensure filling of the microfluidic network. The resulting amperometric signal corresponds to a fasted state. Current values in the lower portion of the detection range were measured, at 830 nA, with a corresponding concentration of 37 μM, according to sensor calibration. After a high calory meal, a second sweat stimulation was performed, 30 minutes after the ingestion, and after a total period of 40 minutes (considering the 10 minutes iontophoresis stimulation), a second amperometric measurement was taken. The reason for this timing is related to the glucose metabolism and the time needed for glucose to reach the blood stream, as well as the lag time between the transference of glucose between blood and other circulating fluids, which in the case of sweat, has been estimated to be 10–20 minutes.[44,45] The resulting current shows a marked increase, to levels around 1.4 μA, corresponding to a glucose level of 234 μM. A second device was assembled with a sensor taken from a new fabrication batch, showing similar results (Fig. S2, ESI†), although the baseline current taken at a fasted state situating below the levels established in the calibration curve. However, once again, the increased current after a meal was recorded, showing that the sensor points to the trend of increasing glucose levels.

3. Conclusions

This work demonstrates the ability to rationally modify paper substrates and employ DLW for high efficiency patterning of low-defect density, high electrical conductivity LIG, compatible for patterning of conformable bioelectrodes for iontophoretic stimulation and electrochemical sensors for sweat biosensing. The transfer of paper-derived LIG through the water-induced peel-off method generates flexible soft conductors on PU substrates, retaining the original conductive characteristics of LIG and enables the modular assembly of iontophoresis electrodes, epifluidics and high-sensitivity sweat glucose biosensors. Iontophoretic delivery of carbachol generated compatible volumes of sweat for up to 1 hour with a single stimulation period, resulting in volumes ranging from 30 to 60 μL, depending on the stimulation current delivered to the skin. The integration of the sweat glucose biosensor demonstrates the capability of quantifying glycemia in sweat by distinguishing fasted and post-prandial states. Due to the ease of form-factor change provided by laser processing fabrication, recent trends in iontophoresis devices for sweat analyte sensing can be followed, including device miniaturization, control of delivery currents for higher-frequency sampling and quantification and rational design of epifluidic modules for efficient sweat collection and transportation. More sustainable devices for automatic sweat stimulation and collection can be envisioned, along with reconfiguration of biosensing schemes for other sweat analytes, self-calibration features for adjustment related to pH or temperature and translational efforts to strengthen the data retrieved using LIG-based wearable biochemical sensing systems.

Author contributions

T. P. conceptualized the idea, conducted overall experiments, performed data analysis, aided in visualization and wrote the manuscript. H. V. A. supervised the research and provided feedback on experiments and hydrogel preparation. D. N. participated in data curation, analysis and visualization of TEM data. R. M. participated in resources and funding acquisition. E. F. conceptualized the idea, supervised the research, resources and funding acquisition. All authors participated in the discussion and revision of the manuscript.

Conflicts of interest

The authors declare no conflicts of interest.

Data availability

All data are shown in the manuscript and the ESI.† The raw data files acquired from instruments are available from the authors.

Acknowledgements

This work was partially financed by FEDER funds through the COMPETE 2020 Programme and the National funds from FCT - Fundação *para* a Ciência e a Tecnologia, I. P., in the scope of projects LA/P/0037/2020, UIDP/50025/2020 and UIDB/50025/2020 of the Associate Laboratory Institute of Nanostructures, Nanomodelling and Nanofabrication – i3N. This work was also partially supported by the European Union's Horizon 2020 Research and Innovation Programme under Grant 101008701 (EMERGE, H2020-INFRAIA-2020-1). We also thank Hiroaki Matsumoto and Akinari Hanawa from Hitachi Hightech Japan for the TEM analysis.

References

1 S. Lee, X. Liang, J. S. Kim, T. Yokota, K. Fukuda and T. Someya, Permeable Bioelectronics toward Biointegrated Systems, *Chem. Rev.*, 2024, **124**(10), 6543–6591, DOI: 10.1021/acs.chemrev.3c00823.

2 L. Cheng, J. Li, A. Guo and J. Zhang, Recent Advances in Flexible Noninvasive Electrodes for Surface Electromyography Acquisition, *npj Flex. Electron.*, 2023, **7**(1), 39, DOI: 10.1038/s41528-023-00273-0.

3 C. Wang, C. Wang, Z. Huang and S. Xu, Materials and Structures toward Soft Electronics, *Adv. Mater.*, 2018, **30**(50), 1801368, DOI: 10.1002/adma.201801368.

4 I. Gablech and E. D. Głowacki, State-of-the-Art Electronic Materials for Thin Films in Bioelectronics, *Adv. Electron. Mater.*, 2023, **9**(8), 2300258, DOI: 10.1002/aelm.202300258.

5 T. Cole, K. Khoshmanesh and S.-Y. Tang, Liquid Metal Enabled Biodevices, *Adv. Intell. Syst.*, 2021, **3**(7), 2000275, DOI: 10.1002/aisy.202000275.

6 Y. Zhang, Y. Liu, Y. Lu, S. Gong, H. Haick, W. Cheng and Y. Wang, Tailor-Made Gold Nanomaterials for Applications in Soft Bioelectronics and Optoelectronics, *Adv. Mater.*, 2024, **36**(36), 2405046, DOI: 10.1002/adma.202405046.

7 X. Gao, Y. Bao, Z. Chen, J. Lu, T. Su, L. Zhang and J. Ouyang, Bioelectronic Applications of Intrinsically Conductive Polymers, *Adv. Electron. Mater.*, 2023, **9**(10), 2300082, DOI: 10.1002/aelm.202300082.

8 H. Yuk, B. Lu and X. Zhao, Hydrogel Bioelectronics, *Chem. Soc. Rev.*, 2019, **48**(6), 1642–1667, DOI: 10.1039/C8CS00595H.

9 S. K. Rastogi, A. Kalmykov, N. Johnson and T. Cohen-Karni, Bioelectronics with Nanocarbons, *J. Mater. Chem. B*, 2018, **6**(44), 7159–7178, DOI: 10.1039/C8TB01600C.

10 S. Baik, H. J. Lee, D. W. Kim, J. W. Kim, Y. Lee and C. Pang, Bioinspired Adhesive Architectures: From Skin Patch to Integrated Bioelectronics, *Adv. Mater.*, 2019, **31**(34), 1803309, DOI: 10.1002/adma.201803309.

11 S. Kumar Das, K. K. Nayak, P. R. Krishnaswamy, V. Kumar and N. Bhat, Review—Electrochemistry and Other Emerging Technologies for Continuous Glucose Monitoring Devices, *ECS Sens. Plus*, 2022, **1**(3), 031601, DOI: 10.1149/2754-2726/ac7abb.

12 G. Kim, H. Ahn, J. Chaj Ulloa and W. Gao, Microneedle Sensors for Dermal Interstitial Fluid Analysis, *Med-X*, 2024, **2**(1), 15, DOI: 10.1007/s44258-024-00028-0.

13 S. M. Khor, J. Choi, P. Won and S. H. Ko, Challenges and Strategies in Developing an Enzymatic Wearable Sweat Glucose Biosensor as a Practical Point-Of-Care Monitoring Tool for Type II Diabetes, *Nanomaterials*, 2022, **12**(2), 221, DOI: 10.3390/nano12020221.

14 H. Lee, Y. J. Hong, S. Baik, T. Hyeon and D. Kim, Enzyme-Based Glucose Sensor: From Invasive to Wearable Device, *Adv. Healthcare Mater.*, 2018, **7**(8), 1701150, DOI: 10.1002/adhm.201701150.

15 S. Emaminejad, W. Gao, E. Wu, Z. A. Davies, H. Y. Y. Nyein, S. Challa, S. P. Ryan, H. M. Fahad, K. Chen, Z. Shahpar, S. Talebi, C. Milla, A. Javey and R. W. Davis, Autonomous Sweat Extraction and Analysis Applied to Cystic Fibrosis and Glucose Monitoring Using a Fully Integrated Wearable Platform, *Proc. Natl. Acad. Sci. U. S. A.*, 2017, **114**(18), 4625–4630, DOI: 10.1073/pnas.1701740114.

16 H. Y. Y. Nyein, W. Gao, Z. Shahpar, S. Emaminejad, S. Challa, K. Chen, H. M. Fahad, L.-C. Tai, H. Ota, R. W. Davis and A. Javey, A Wearable Electrochemical Platform for Noninvasive Simultaneous Monitoring of Ca 2+ and PH, *ACS Nano*, 2016, **10**(7), 7216–7224, DOI: 10.1021/acsnano.6b04005.

17 Y. Yang, Y. Song, X. Bo, J. Min, O. S. Pak, L. Zhu, M. Wang, J. Tu, A. Kogan, H. Zhang, T. K. Hsiai, Z. Li and W. Gao, A Laser-Engraved Wearable Sensor for Sensitive Detection of Uric Acid and Tyrosine in Sweat, *Nat. Biotechnol.*, 2020, **38**(2), 217–224, DOI: 10.1038/s41587-019-0321-x.

18 J. Tu, J. Min, Y. Song, C. Xu, J. Li, J. Moore, J. Hanson, E. Hu, T. Parimon, T.-Y. Wang, E. Davoodi, T.-F. Chou, P. Chen, J. J. Hsu, H. B. Rossiter and W. Gao, A Wireless Patch for the Monitoring of C-Reactive Protein in Sweat, *Nat. Biomed. Eng.*, 2023, **7**(10), 1293–1306, DOI: 10.1038/s41551-023-01059-5.

19 R. M. Torrente-Rodríguez, J. Tu, Y. Yang, J. Min, M. Wang, Y. Song, Y. Yu, C. Xu, C. Ye, W. W. IsHak and W. Gao, Investigation of Cortisol Dynamics in Human Sweat Using a Graphene-Based Wireless MHealth System, *Matter*, 2020, **2**(4), 1–17, DOI: 10.1016/j.matt.2020.01.021.

20 K. Xu, Z. Cai, H. Luo, Y. Lu, C. Ding, G. Yang, L. Wang, C. Kuang, J. Liu and H. Yang, Toward Integrated Multifunctional Laser-Induced Graphene-Based Skin-Like Flexible Sensor Systems, *ACS Nano*, 2024, **18**(39), 26435–26476, DOI: 10.1021/acsnano.4c09062.

21 M. Sharifuzzaman, M. A. Zahed, M. S. Reza, M. Asaduzzaman, S. H. Jeong, H. Song, D. K. Kim, S. Zhang and J. Y. Park, MXene/Fluoropolymer-Derived Laser-Carbonaceous All-Fibrous Nanohybrid Patch for Soft Wearable Bioelectronics, *Adv. Funct. Mater.*, 2023, **33**(21), 2208894, DOI: 10.1002/adfm.202208894.

22 N. T. Garland, J. Schmieder, Z. T. Johnson, R. G. Hjort, B. Chen, C. Andersen, D. Sanborn, G. Kjeldgaard, C. C. Pola, J. Li, C. Gomes, E. A. Smith, H. Angus, J. Meyer and J. C. Claussen, Wearable Flexible Perspiration Biosensors Using Laser-Induced Graphene and Polymeric Tape Microfluidics, *ACS Appl. Mater. Interfaces*, 2023, **15**(32), 38201–38213, DOI: **10.1021/acsami.3c04665**.

23 F. Lorestani, X. Zhang, A. M. Abdullah, X. Xin, Y. Liu, M. M. Rahman, M. A. S. Biswas, B. Li, A. Dutta, Z. Niu, S. Das, S. Barai, K. Wang and H. Cheng, A Highly Sensitive and Long-Term Stable Wearable Patch for Continuous Analysis of Biomarkers in Sweat, *Adv. Funct. Mater.*, 2023, **33**(52), 2306117, DOI: **10.1002/adfm.202306117**.

24 H. Sun, S. Song, G. Zhao, X. Wang and G. Liu, A Flexible and Wearable Chemiresistive Biosensor Fabricated by Laser Inducing for Real-Time Glucose Analysis of Sweat, *Adv. Mater. Interfaces*, 2023, **10**(22), 2300281, DOI: **10.1002/admi.202300281**.

25 Y. Wang, H. Guo, M. Yuan, J. Yu, Z. Wang and X. Chen, One-Step Laser Synthesis Platinum Nanostructured 3D Porous Graphene: A Flexible Dual-Functional Electrochemical Biosensor for Glucose and PH Detection in Human Perspiration, *Talanta*, 2023, **257**, 124362, DOI: **10.1016/j.talanta.2023.124362**.

26 J. Zhu, S. Liu, Z. Hu, X. Zhang, N. Yi, K. Tang, M. G. Dexheimer, X. Lian, Q. Wang, J. Yang, J. Gray and H. Cheng, Laser-Induced Graphene Non-Enzymatic Glucose Sensors for on-Body Measurements, *Biosens. Bioelectron.*, 2021, **193**, 113606, DOI: **10.1016/j.bios.2021.113606**.

27 Z. Zhang, L. Huang, Y. Chen, Z. Qiu, X. Meng and Y. Li, Portable Glucose Sensing Analysis Based on Laser-Induced Graphene Composite Electrode, *RSC Adv.*, 2024, **14**(2), 1034–1050, DOI: **10.1039/D3RA06947H**.

28 H. Yoon, J. Nah, H. Kim, S. Ko, M. Sharifuzzaman, S. C. Barman, X. Xuan, J. Kim and J. Y. Park, A Chemically Modified Laser-Induced Porous Graphene Based Flexible and Ultrasensitive Electrochemical Biosensor for Sweat Glucose Detection, *Sens. Actuators, B*, 2020, **311**, 127866, DOI: **10.1016/j.snb.2020.127866**.

29 Y. Luo, B. Zhu, S. Zhang, P. Zhang, X. Li, L. Wang, B. Lu and J. Travas-Sejdic, Stretchable and Flexible Non-Enzymatic Glucose Sensor Based on Poly(Ether Sulfone)-Derived Laser-Induced Graphene for Wearable Skin Diagnostics, *Adv. Mater. Technol.*, 2022, **7**(9), 2101571, DOI: **10.1002/admt.202101571**.

30 Y. Lei, A. H. Alshareef, W. Zhao and S. Inal, Laser-Scribed Graphene Electrodes Derived from Lignin for Biochemical Sensing, *ACS Appl. Nano Mater.*, 2020, **3**(2), 1166–1174, DOI: **10.1021/acsanm.9b01795**.

31 M. Wang, Y. Yang, J. Min, Y. Song, J. Tu, D. Mukasa, C. Ye, C. Xu, N. Heflin, J. S. McCune, T. K. Hsiai, Z. Li and W. Gao, A Wearable Electrochemical Biosensor for the Monitoring of Metabolites and Nutrients, *Nat. Biomed. Eng.*, 2022, **6**(11), 1225–1235, DOI: **10.1038/s41551-022-00916-z**.

32 P. Simmers, S. K. Li, G. Kasting and J. Heikenfeld, Prolonged and Localized Sweat Stimulation by Iontophoretic Delivery of the Slowly-Metabolized Cholinergic Agent Carbachol, *J. Dermatol. Sci.*, 2018, **89**(1), 40–51, DOI: **10.1016/j.jdermsci.2017.10.013**.

33 T. Pinheiro, R. Correia, M. Morais, J. Coelho, E. Fortunato, M. G. F. Sales, A. C. Marques and R. Martins, Water Peel-Off Transfer of Electronically Enhanced, Paper-Based Laser-Induced Graphene for Wearable Electronics, *ACS Nano*, 2022, **16**(12), 20633–20646, DOI: **10.1021/acsnano.2c07596**.

34 J. Lin, Z. Peng, Y. Liu, F. Ruiz-Zepeda, R. Ye, E. L. G. Samuel, M. J. Yacaman, B. I. Yakobson and J. M. Tour, Laser-Induced Porous Graphene Films from Commercial Polymers, *Nat. Commun.*, 2014, **5**(1), 5714, DOI: **10.1038/ncomms6714**.

35 A. Ghosh, S. Kaur, G. Verma, C. Dolle, R. Azmi, S. Heissler, Y. M. Eggeler, K. Mondal, D. Mager, A. Gupta, J. G. Korvink, D.-Y. Wang, A. Sharma and M. Islam, Enhanced Performance of Laser-Induced Graphene Supercapacitors via Integration with Candle-Soot Nanoparticles, *ACS Appl. Mater. Interfaces*, 2024, **16**(31), 40313–40325, DOI: **10.1021/acsami.4c07094**.

36 D. Nunes, M. Vilarigues, J. B. Correia and P. A. Carvalho, Nickel–Carbon Nanocomposites: Synthesis, Structural Changes and Strengthening Mechanisms, *Acta Mater.*, 2012, **60**(2), 737–747, DOI: **10.1016/j.actamat.2011.10.012**.

37 L. Cheng, C. S. Yeung, L. Huang, G. Ye, J. Yan, W. Li, C. Yiu, F.-R. Chen, H. Shen, B. Z. Tang, Y. Ren, X. Yu and R. Ye, Flash Healing of Laser-Induced Graphene, *Nat. Commun.*, 2024, **15**(1), 2925, DOI: **10.1038/s41467-024-47341-1**.

38 A. K. Banga, S. Bose and T. K. Ghosh, Iontophoresis and Electroporation: Comparisons and Contrasts, *Int. J. Pharm.*, 1999, **179**(1), 1–19, DOI: **10.1016/S0378-5173(98)00360-3**.

39 H. Hojaiji, Y. Zhao, M. C. Gong, M. Mallajosyula, J. Tan, H. Lin, A. M. Hojaiji, S. Lin, C. Milla, A. M. Madni and S. Emaminejad, An Autonomous Wearable System for Diurnal Sweat Biomarker Data Acquisition, *Lab Chip*, 2020, **20**(24), 4582–4591, DOI: **10.1039/D0LC00820F**.

40 J. Kim, I. Jeerapan, S. Imani, T. N. Cho, A. Bandodkar, S. Cinti, P. P. Mercier and J. Wang, Noninvasive Alcohol Monitoring Using a Wearable Tattoo-Based Iontophoretic-Biosensing System, *ACS Sens.*, 2016, **1**(8), 1011–1019, DOI: **10.1021/acssensors.6b00356**.

41 J. R. Sempionatto, A. A. Khorshed, A. Ahmed, E. De Loyola, A. N. Silva, A. Barfidokht, L. Yin, K. Y. Goud, M. A. Mohamed, E. Bailey, J. May, C. Aebischer, C. Chatelle and J. Wang, Epidermal Enzymatic Biosensors for Sweat Vitamin C: Toward Personalized Nutrition, *ACS Sens.*, 2020, **5**(6), 1804–1813, DOI: **10.1021/acssensors.0c00604**.

42 G. Bolat, E. De la Paz, N. F. Azeredo, M. Kartolo, J. Kim, A. N. de Loyola e Silva, R. Rueda, C. Brown, L. Angnes, J. Wang and J. R. Sempionatto, Wearable Soft Electrochemical Microfluidic Device Integrated with Iontophoresis for Sweat Biosensing, *Anal. Bioanal. Chem.*, 2022, **414**(18), 5411–5421, DOI: **10.1007/s00216-021-03865-9**.

43 A. Hauke, P. Simmers, Y. R. Ojha, B. D. Cameron, R. Ballweg, T. Zhang, N. Twine, M. Brothers, E. Gomez and J. Heikenfeld, Complete Validation of a Continuous and Blood-Correlated Sweat Biosensing Device with

Integrated Sweat Stimulation, *Lab Chip*, 2018, **18**(24), 3750–3759, DOI: **10.1039/C8LC01082J**.

44 T. D. La Count, A. Jajack, J. Heikenfeld and G. B. Kasting, Modeling Glucose Transport From Systemic Circulation to Sweat, *J. Pharm. Sci.*, 2019, **108**(1), 364–371, DOI: **10.1016/j.xphs.2018.09.026**.

45 T. Saha, M. I. Khan, S. S. Sandhu, L. Yin, S. Earney, C. Zhang, O. Djassemi, Z. Wang, J. Han, A. Abdal, S. Srivatsa, S. Ding and J. Wang, A Passive Perspiration Inspired Wearable Platform for Continuous Glucose Monitoring, *Adv. Sci.*, 2024, 2405518, DOI: **10.1002/advs.202405518**.